

# Nonlinear Outcome of Gravitational Instability in Cooling, Gaseous Disks

Charles F. Gammie

*Center for Theoretical Astrophysics,*

*Physics Department, and Astronomy Department*

*University of Illinois at Urbana-Champaign*

*1110 W. Green St.*

*Urbana, IL 61801*

## ABSTRACT

Thin, Keplerian accretion disks generically become gravitationally unstable at large radius. I investigate the nonlinear outcome of such instability in cool disks using razor-thin, local, numerical models. Cooling, characterized by a constant cooling time  $\tau_c$ , drives the instability.

I show analytically that, if the disk can reach a steady state in which heating by dissipation of turbulence balances cooling, then the dimensionless angular momentum flux density  $\alpha = ((9/4)\gamma(\gamma - 1)\Omega\tau_c)^{-1}$ . Numerical experiments show that: (1) if  $\tau_c \gtrsim 3\Omega^{-1}$  then the disk reaches a steady, gravito-turbulent state in which  $Q \sim 1$  and cooling is balanced by heating due to dissipation of turbulence; (2) if  $\tau_c \lesssim 3\Omega^{-1}$ , then the disk fragments, possibly forming planets or stars; (3) in a steady, gravito-turbulent state, surface density structures have a characteristic physical scale  $\sim 64G\Sigma/\Omega^2$  that is independent of the size of the computational domain.

*Subject headings:* accretion, accretion disks, solar system: formation, galaxies: nuclei

## 1. Introduction

It has long been realized that the outer reaches of accretion disks around active galactic nuclei (AGN) and young stellar objects (YSO) may be gravitationally unstable (for a review see, for AGN: Shlosman et al. (1990); YSOs: Adams & Lin (1993)). Instability in a Keplerian disk sets in where the sound speed  $c_s$ , the rotation frequency  $\Omega$ , and the surface density  $\Sigma$  satisfy

$$Q \equiv \frac{c_s \Omega}{\pi G \Sigma} < Q_{crit} \simeq 1 \quad (1)$$

(Toomre 1964; Goldreich & Lynden-Bell 1965). Here  $Q_{crit} = 1$  for a “razor-thin” (two dimensional) fluid disk, and  $Q_{crit} = 0.676$  for a finite thickness isothermal disk (Goldreich & Lynden-Bell 1965).

The instability condition (1) can be rewritten, for a disk with scale height  $H \simeq c_s/\Omega$ , around a central object of mass  $M_*$ ,

$$M_{disk} \gtrsim \frac{H}{r} M_*, \quad (2)$$

where  $M_{disk} \equiv \pi r^2 \Sigma$ .

In a steady-state disk whose heating is dominated by interior turbulent dissipation and whose evolution is controlled by internal transport of angular momentum, the accretion rate  $\dot{M} = 3\pi\alpha c_s^2 \Sigma/\Omega$ , where I have used the  $\alpha$  formalism of Shakura & Sunyaev (1973). Then

$$\dot{M} \gtrsim \frac{3\alpha c_s^3}{G} = 7.1 \times 10^{-4} \alpha \left( \frac{c_s}{1 \text{ km s}^{-1}} \right)^3 \text{ M}_\odot \text{ yr}^{-1} \quad (3)$$

implies gravitational instability (e.g. Shlosman et al. (1990)). This does not apply to disks dominated by external torques (e.g., a magnetohydrodynamic [MHD] wind) or disks heated mainly by external illumination.

For a young, solar mass star accreting from a disk with  $\alpha = 10^{-2}$  at  $10^{-6} \text{ M}_\odot \text{ yr}^{-1}$  equation (3) implies that instability occurs where the temperature drops below 17 K. Disks may not be this cold if the star is located in a warm molecular cloud where the ambient temperature is greater than 17 K, or if the disk is bathed in scattered infrared light from the central star (although there is some evidence for such low temperatures in the solar nebula, e.g. Owen et al. (1999)). If the effective value of  $\alpha$  is small and heating is confined to surface layers, however, as in the layered accretion model of Gammie (1996a), then instability can occur at much higher temperatures.

AGN disk heating is typically dominated by illumination from a central source. The temperature then depends on the shape of the disk. If the disk is flat or shadowed, however, and transport is dominated by internal torques, one can apply equation (3). For example, in the nucleus of NGC 4258 (Miyoshi et al. 1995) the accretion rate may be as large as  $10^{-2} \text{ M}_\odot \text{ yr}^{-1}$  (Lasota et al. 1996; Gammie et al. 1999). Equation (3) then implies that instability sets in where  $T < 10^4(\alpha/10^{-2}) \text{ K}$ . If the disk is illumination-dominated, however, then  $Q$  fluctuates with the luminosity of the central source.

The fate of a gravitationally unstable YSO or AGN disk depends on how it arrived in an unstable state. To understand why, consider an analogy with convective instability in stellar structure theory. The evolution of stellar models with highly unstable radial entropy profiles are of little interest, because convection prevents such models from being realized in an astrophysically plausible setting. Similarly, highly unstable disks may be irrelevant because the action of the instability would prevent one from ever arriving in such a state. Gravitational instability must be “turned on” in a natural way.

An initially stable Keplerian disk can be driven unstable by an increase in surface density (e.g. Sellwood & Carlberg (1984)) or by cooling. In an  $\alpha$  disk model, the surface density changes on the accretion timescale  $\sim (r/H)^2(\alpha\Omega)^{-1}$  (more rapid variation of surface density could be obtained by dumping material onto the disk or by application of a direct magnetic torque). The temperature,

by contrast, changes on the cooling time,  $\sim (\alpha\Omega)^{-1}$ . This suggests that in cool disks ( $r/H \gg 1$ ), cooling is the dominant driver of gravitational instability.

Once gravitational instability sets in, the disk can attempt to regain stability by rearranging its mass to reduce  $\Sigma$ , or by heating itself through dissipation of turbulence. Dissipation can occur directly through shocks or indirectly via a turbulent cascade to the viscous scale. If one can model the effects of “gravito-turbulence” on a cool disk as an  $\alpha$  viscosity, then mass shifting can be accomplished only on the accretion timescale  $(r/H)^2(\alpha\Omega)^{-1}$ . Heating occurs on the thermal timescale  $(\alpha\Omega)^{-1}$ . This suggests that cool disks will attempt to reestablish stability through dissipation of turbulence.

Let us assume that cooling drives the disk toward instability, and that the disk tries to recover through turbulent dissipation. There is now the possibility of a feedback loop. If  $Q$  is too large then heating by gravito-turbulence is weak and the disk cools toward instability. If  $Q$  is too small, heating by gravito-turbulence is strong and the disk is pushed back toward marginal stability. The feedback loop acts as a thermostat to maintain  $Q \sim 1$ , just as convection in stars drives the entropy profile toward marginal stability.

The effectiveness of the feedback loop in maintaining  $Q \sim 1$  is controversial. Lin & Pringle (1987, 1990) have considered disk models with  $Q \ll 1$ . Indeed it is not clear that the feedback is strong enough to preserve  $Q \sim 1$ . Cooling might be so rapid that the disk fragments before it can heat (Shlosman & Begelman 1989), leading to formation of gas giant planets or stars.

The feedback loop is an old idea in the theory of galactic disks (Goldreich & Lynden-Bell (1965); there heating due to star formation balances cooling) and in accretion disk theory (Paczynski 1978). Numerical experiments on cooled collisionless disk models (Anthony & Carlberg 1988; Carlberg & Freedman 1985; Tomley et al. 1991, 1994) do yield disks with  $Q \sim 1$ , and clumping with sufficiently strong cooling. Observations of star forming regions of galactic disks also show  $Q \sim 1$  in the gas (Kennicutt 1989).

Numerical experiments with fluid disks often assume a fixed temperature profile or a fixed entropy profile (Boss 1997, 1998; Nelson et al. 1998). A fixed temperature profile is relevant to an illumination-dominated disk. Other work considers the adiabatic evolution of an initially unstable state (Pickett et al. 2000; Laughlin & Różyczka 1996; Yang et al. 1991). Recent work by Nelson et al. (2000) is most comparable to that presented here. It examines the evolution of cooling, global models of the disks, but with a more complicated treatment of the cooling function.

In this paper I consider the nonlinear evolution of cooling, self-gravitating fluid disks via numerical experiment. The disk model is razor-thin (two dimensional) and local. In §2 I describe the model, then show that its angular momentum flux density can be calculated analytically (§3), provided that the disk does not fragment. The results of numerical experiments are described in §4. Conclusions are given in §5.

## 2. Model

The direct, numerical evolution of a global self-gravitating disk model over many dynamical times is prohibitively expensive. To develop a converged, calculable, numerical model, and to reduce the number of free parameters associated with a global disk model, I make two simplifying assumptions: that the disk is cool (i.e. thin, so  $H/r \simeq c_s/(\Omega r) \ll 1$ ) and that it razor-thin.

A cool disk can be modeled using a rigorous expansion of the equations of motion through lowest order in  $c_s/(\Omega r)$ . This model is called the “local model” or “shearing sheet.” The expansion proceeds as follows. Choose a fiducial point  $(r_o, \phi_o + \Omega(r_o)t)$  that corotates with the disk. Define a set of local Cartesian coordinates  $x, y \equiv r - r_o, r_o(\phi - \phi_o - \Omega(r_o)t)$ , and expand the equations of motion to first order in  $|x|/r_o$ . To do this, one needs to assume that the departures from circular orbits in the disk  $|\delta\mathbf{v}| \sim c_s \ll \Omega r_o$ , and similarly that the perturbed potential  $\delta\phi \sim c_s^2 \ll (\Omega r_o)^2$ . With this assumption, the local model describes the evolution of the disk near the fiducial point. The self-consistency of these orderings can be tested in the nonlinear evolution.

I will also use a “razor-thin” disk approximation that treats the disk as two dimensional. There is good agreement between razor-thin models and full three dimensional evolution in the linear theory of polytropic slender tori (Goldreich et al. 1986), in nonlinear simulations of polytropic tori (Hawley 1990), and in nonlinear simulations of gas flow in spiral arms with an isothermal equation of state (Tubbs 1980). In general there can be no rigorous mapping between razor-thin disks and full three-dimensional systems because the vertical structure contains degrees of freedom that are absent in the razor-thin model.

The equations of motion in the local model read, where  $\mathbf{v}$  is the velocity,  $P$  is the (two-dimensional) pressure, and  $\phi$  is the gravitational potential with the time-steady axisymmetric component removed:

$$\frac{D\mathbf{v}}{Dt} = -\frac{\nabla P}{\Sigma} - 2\boldsymbol{\Omega} \times \mathbf{v} + 3\Omega^2 x \hat{\mathbf{e}}_x - \nabla\phi. \quad (4)$$

For constant pressure and surface density,  $\mathbf{v} = -\frac{3}{2}\Omega x \hat{\mathbf{e}}_y$  is an equilibrium solution to the equations of motion. This linear shear flow is the manifestation of differential rotation in the local model.

The equation of state is

$$P = (\gamma - 1)U, \quad (5)$$

where  $P$  is the two-dimensional pressure and  $U$  the two-dimensional internal energy. I will adopt  $\gamma = 2$  throughout. The two dimensional (2D) adiabatic index  $\gamma$  can be mapped to a 3D adiabatic index  $\Gamma$  in the low-frequency (static) limit. For a nonself-gravitating disk  $\gamma = (3\Gamma - 1)/(\Gamma + 1)$  (e.g. Goldreich et al. 1986, Ostriker et al. 1992). For a strongly self-gravitating disk, one can show that  $\gamma = 3 - 2/\Gamma$ .

If the evolution is strictly adiabatic and the initial conditions are isentropic, then  $p = K\Sigma^\gamma$  with  $K = \text{const}$ . It follows that the “potential vorticity”

$$\xi \equiv \frac{\nabla \times \mathbf{v} + 2\boldsymbol{\Omega}}{\Sigma} \quad (6)$$

obeys  $D\xi/Dt = 0$ . There is a close connection between the conservation of potential vorticity and the stabilizing effects of rotation (Lynden-Bell 1966; Hunter 1964). Processes that cause the potential vorticity to evolve can compromise rotational support of the disk at long wavelengths (Gammie 1996b).

The internal energy equation is

$$\frac{\partial U}{\partial t} + \nabla \cdot (U\mathbf{v}) = -P\nabla \cdot \mathbf{v} - \frac{U}{\tau_c} \quad (7)$$

The final term is the cooling function, and  $\tau_c$  is the cooling time. In general  $\tau_c = \tau_c(\Sigma, U, \Omega)$ . I will make the simplifying assumption that  $\tau_c = \text{const}$ . Notice that there is no heating term; heating is due solely to shocks. Numerically, the fluid is heated by artificial viscosity in shocks.

The gravitational potential is determined by the razor-thin disk Poisson equation:

$$\nabla^2 \phi = 4\pi G \Sigma \delta(z). \quad (8)$$

For a single Fourier component of the surface density  $\Sigma_{\mathbf{k}}$  this has the solution

$$\phi = -\frac{2\pi G}{|\mathbf{k}|} \Sigma_{\mathbf{k}} e^{i\mathbf{k}\cdot\mathbf{x} - |kz|}. \quad (9)$$

A finite thickness disk has weaker self-gravity, but this does not qualitatively change the dynamics of the disk in linear theory (Goldreich & Lynden-Bell 1965).

## 2.1. Boundary Conditions, Numerical Methods, and Tests

I use the “shearing box” boundary conditions, described in detail by Hawley et al. (1995). They apply to a rectangular domain of size  $L_x$  by  $L_y$ , although I will assume, unless stated otherwise, that  $L_x = L_y \equiv L$ . The boundary conditions may be written, for dependent variable  $f = (\Sigma, U, v_x, \delta v_y \equiv v_y + \frac{3}{2}\Omega x)$ ,

$$f(x, y) = f(x, y + L) \quad (10)$$

$$f(x, y) = f(x + L, y - \frac{3}{2}\Omega L t) \quad (11)$$

These boundary conditions have been used to study accretion disks (Hawley et al. 1995), galactic disks (Toomre & Kalnajs 1991), and planetary rings (Wisdom & Tremaine 1988).

I integrate the governing equations using a self-gravitating hydrodynamics code based on ZEUS (Stone & Norman 1992). ZEUS is a time-explicit, operator-split, finite-difference method on a staggered mesh. It uses an artificial viscosity to capture shocks. My implementation has been tested on standard linear and nonlinear problems, such as sound waves and shock tubes, with acceptable results.

The transport scheme differs significantly from the basic ZEUS algorithm. I divide the transport step into two pieces: one due to the mean velocity  $-\frac{3}{2}\Omega x \hat{\mathbf{e}}_y$  and the other due to the remaining, perturbed velocity. The mean velocity transport is done by linear interpolation, while the perturbed velocity transport is done as in ZEUS.<sup>1</sup> The “ghost zones” outside the boundaries are likewise set using linear interpolation. This algorithm has the advantage that the timestep is limited not by the large shear velocity at the radial edges of the grid,  $-\frac{3}{2}\Omega(L/2)$ , but by the perturbed velocities only. Longer timesteps can therefore be used, and numerical diffusion is reduced and more nearly uniform across the grid.

I solve the Poisson equation using the Fourier transform method, modified for the shearing box boundary conditions. The density is periodic in shearing coordinates  $x, y'$ , where

$$y' = y - \frac{3}{2}\Omega x(t - t_p) \quad (12)$$

and  $t_p = (\frac{3}{2}\Omega)^{-1} \text{NINT}(t \frac{3}{2}\Omega)$ . Thus when  $t = t_p$ , which happens at intervals  $\Delta t = (\frac{3}{2}\Omega)^{-1}$ , the model is periodic in  $x, y$ . I linearly interpolate  $\Sigma$  onto a grid in  $x, y'$ , solve for the potential via Fourier transform, linearly interpolate the potential back onto a grid in  $x, y$ , and then difference to obtain the acceleration.

There is one subtlety involved in the solution of the Poisson equation. In the Fourier domain, the grid of available wavenumbers forms a parallelogram in the  $k_x, k_y$  plane whose shape changes with time. I use only those wavenumbers with  $|\mathbf{k}| < (2)^{-1/2}(N/2)(2\pi/L)$  in the solution, where  $N \times N$  is the numerical resolution of the model. This restricts the gravitational kernel to the largest circular region in Fourier space that is always available. This restriction ensures that the gravitational force is approximately isotropic on small scales.

I have tested my algorithm on three problems. First, I tested the transport piece of the code. I evolved, for one rotation period, initial conditions in which  $v_x(t=0) = \text{const.}$ ,  $P = 0$ , and a square of enhanced density was placed in the middle of the grid. The square sheared out, crossed a radial boundary, and returned to its initial position. The density enhancement diffused somewhat, but no features were introduced at the boundary crossing. Second, I tested the code’s ability to conserve potential vorticity. I evolved initial conditions containing a sinusoidal velocity perturbation for several shear times. Only modest diffusion of potential vorticity was observed. Finally, I checked the evolution of a sinusoidal density perturbation against linear theory.

A comparison of code output with linear theory is shown in Figure 1. The test model has  $L = 40G\Sigma_0/\Omega^2$ ,  $Q = 1$ , and no cooling. The initial conditions are  $\mathbf{v} = -\frac{3}{2}\Omega x \hat{\mathbf{e}}_y$  and  $\Sigma = \Sigma_0 + \delta\Sigma \cos(\mathbf{k} \cdot \mathbf{x})$ , with  $k_x = -2(2\pi/L)$ ,  $k_y = (2\pi/L)$ , and  $\delta\Sigma/\Sigma_0 = 5 \times 10^{-4}$ . Linear theory (see Gammie (1996b), and references therein) gives the evolution of the amplitude  $\delta\Sigma(t)$  of a shearing wave  $\cos(\mathbf{k} \cdot \mathbf{x})$  where  $k_x(t) = k_x(0) + \frac{3}{2}\Omega k_y t$  and  $k_y = \text{const.}$ . The heavy solid line in the figure shows the linear theory result. The other lines show the evolution of the test models, which start

---

<sup>1</sup>I thank J. Goodman for suggesting this. See also Masset (1999).

at  $N = 32$  (poorest agreement with linear theory) and run by factors of 2 up to  $N = 256$ . Since the radial wavenumber of the disturbance increases with time, the wave eventually becomes wrapped up and unresolved. At the end of the run ( $t = 10\Omega^{-1}$ ) the radial wavelength is  $L/13$ , or  $2.46 \times (N/32)$  zones. Evidently the numerical integration converges on the linear theory result.

### 3. Analytical Properties of the Model

Consider the following Jacobi-like “integral” for the shearing box:

$$\Gamma = \int d^3\mathbf{x} \Sigma \delta(z) \left( \frac{1}{2}v^2 + \frac{U}{\Sigma} + \phi_T + \frac{1}{2}\phi \right). \quad (13)$$

Here  $\phi_T = -\frac{3}{2}\Omega^2 x^2$  is the tidal expansion of the effective potential about the fiducial point, and  $\phi$  is the potential of surface density fluctuations. The integral is taken over the entire simulation area and from  $z = -\infty$  to  $z = \infty$ . Now evaluate  $\partial\Gamma/\partial t$  using the energy equation, the equations of motion, the Poisson equation, and the boundary conditions:

$$\frac{\partial\Gamma}{\partial t} = \frac{3}{2}\Omega L \int_X dS \left( \Sigma v_x \delta v_y + \frac{g_x g_y}{4\pi G} \right) - \frac{1}{\tau_c} \int d^3\mathbf{x} U \delta(z), \quad (14)$$

where the surface integral is taken over one of the radial boundaries (the azimuthal boundaries do not contribute because they are periodic). To obtain this result, one must realize that terms proportional to  $D\phi/Dt$  vanish when integrated over the boundaries, while terms proportional to  $\partial\phi/\partial t = D\phi/Dt - (\mathbf{v} \cdot \nabla)\phi$  do not.

Now average equation (14) over  $t$ ,  $x$ , and  $y$ , replacing  $\int_X dS f$  by  $L\langle \int dz f \rangle$ . If the disk can settle into a steady state then  $\langle \partial\Gamma/\partial t \rangle = 0$  and

$$\left\langle \Sigma v_x \delta v_y + \int dz \frac{g_x g_y}{4\pi G} \right\rangle = \frac{\langle U \rangle}{\frac{3}{2}\Omega \tau_c}, \quad (15)$$

The left hand side is the shear stress, which is proportional to the angular momentum flux density.

The shear stress can be divided into a hydrodynamic piece and a gravitational piece. The hydrodynamic shear stress is obtained via the usual Reynolds decomposition: the fluid velocity is reduced to the sum of a mean steady part  $-\frac{3}{2}\Omega x \hat{\mathbf{e}}_y$  and a fluctuating part  $v_x \hat{\mathbf{e}}_x + \delta v_y \hat{\mathbf{e}}_y$ . Then the associated “Reynolds stress” is

$$H_{xy} = \Sigma v_x \delta v_y. \quad (16)$$

Notice that the mean radial velocity is of order  $c_s(H/r)^2$ , so in the local model, accurate to first order in  $H/r$ , the mean radial velocity is zero. Thus the local model can be used to calculate a shear stress, but a global model is needed to relate the shear stress to an accretion rate.

The gravitational piece of the shear stress is

$$G_{xy} = \int_{-\infty}^{\infty} dz \frac{g_x g_y}{4\pi G} \quad (17)$$

(Lynden-Bell & Kalnajs 1972). The vertical integral arises because the gravitational field outside the disk contributes to the shear stress. The vertical integral can be done analytically in the Fourier domain, giving the space-averaged gravitational shear stress:

$$\langle G_{xy} \rangle = \sum_{\mathbf{k}} \frac{\pi G k_x k_y |\Sigma_{\mathbf{k}}|^2}{|\mathbf{k}|^3}. \quad (18)$$

The sum is over all Fourier components.

It is convenient to express the shear stress in terms of an effective  $\alpha$ :

$$\alpha \equiv \frac{2}{3 \langle \Sigma c_s^2 \rangle} (G_{xy} + H_{xy}). \quad (19)$$

Using equation (15), and  $U = c_s^2 \Sigma / (\gamma(\gamma - 1))$ , I find

$$\alpha = \left( \gamma(\gamma - 1) \frac{9}{4} \Omega \tau_c \right)^{-1}. \quad (20)$$

For  $\gamma = 2$ ,

$$\alpha = \frac{2}{9} \frac{1}{\Omega \tau_c}. \quad (21)$$

It is remarkable that it is possible to calculate  $\alpha$  analytically for this simple model. Equation (20) does not close the system of equations for disk evolution, however, because in general  $\tau_c$  is a function of the disk temperature. It is the local analog of the result that the surface brightness of the disk is independent of the details of the angular momentum transport mechanism. Fixing  $Q$  would close the system of equations, but  $Q$  is not known *a priori*. This result, however, can serve as a check on numerical work. It also explains the empirical relation between cooling rate and angular momentum flux reported by Tomley et al. (1994).

## 4. Nonlinear Outcome

### 4.1. Standard Run

Consider the evolution of a single “standard” run, with  $L = 320G\Sigma/\Omega^2$  and  $N = 1024$ . The initial velocities are  $v_x = \delta v_x$ ,  $v_y = -\frac{3}{2}\Omega x + \delta v_y$ , where  $\delta \mathbf{v}$  is a white noise random velocity field of subsonic amplitude (the outcome is nearly independent of the details of these perturbations). The initial internal energy is such that  $Q = 1$ , and the cooling time is  $\tau_c = 10\Omega^{-1}$ .

The evolution of the kinetic, gravitational, and thermal energy per unit area, normalized to  $G^2\Sigma^3/\Omega^2$ , are shown in Figure 2. The evolution of the gravitational and hydrodynamic components of  $\alpha$  are shown in Figure 3. The  $\alpha$ ’s have been smoothed to make the plot readable. A snapshot of the surface density at  $t = 50\Omega^{-1}$  is shown as a color plot in Figure 4; red is high density and blue is low density.

As the model evolves the small initial velocity fluctuations grow exponentially and develop into nonlinear surface density, velocity, and potential fluctuations. Shocks of a predominantly trailing orientation develop and heat the gas, while cooling works to reduce the gas entropy. Density structures develop which are sheared out by differential rotation and are also predominantly trailing. The tendency of velocity and density structures to take on a trailing figure gives rise to a finite  $\alpha$ .

Eventually the thermal energy of the disk settles down to a steady state in which the disk is near the point of marginal stability, as hypothesized by Paczyński (1978). The mean stability parameter  $\langle Q \rangle \equiv \langle c_s \rangle \Omega / \pi G \langle \Sigma \rangle$  fluctuates slightly, but averages 2.46 over the last  $80\Omega^{-1}$  of the run. This is larger than the neutrally stable value ( $Q = 1$ ), but small enough that the disk remains sensitive to nonaxisymmetric disturbances. This confirms the hypothesis that the disk maintains  $Q \sim 1$ .

The analytic theory of the last section predicts that  $\alpha = 2/90 \approx 0.022$ . Averaging over the final  $80\Omega^{-1}$  of the run, I find  $\alpha = 0.0247$ . The difference is due to energy nonconservation. Grid scale velocity differences are damped by numerical averaging. That fraction of the energy extracted from the shear that does not go into shocks and shock heating winds up in a turbulent cascade and is lost at the grid scale (one could close the energy equation by introducing a viscosity, but this introduces a new set of dynamical complications that will be treated in a separate publication). The sense of the difference can be understood by noting that  $\alpha$  measures the rate of energy extraction from the shear flow. The extracted energy flows by shock heating into thermal energy of the disk, and from there to cooling. In a steady state, all must balance. If some of the energy is lost before heating the disk, the loss must be compensated for by an increase in the rate of energy extraction.

## 4.2. Effect of Cooling Time

The fates of gravitationally unstable disks can be divided into two classes, depending on the cooling time. I find that for short cooling times,  $\tau_c \lesssim 3\Omega^{-1}$ , the model disk fragments. This is easy to understand: for very short cooling times pieces of the disk cool and collapse before they have an opportunity to collide with one another and reheat the disk (Shlosman & Begelman 1989).

Fragmentation is illustrated in Figure 5, which shows a snapshot from a run with  $N = 512$ ,  $L = 80G\Sigma/\Omega^2$ ,  $\tau_c = 2\Omega^{-1}$ . In this run the disk initially fragments into 6 bound objects, which then undergo collisional agglomeration. Ultimately a single bound object forms which is itself a self-gravitating accretion disk. This disk has a rotation frequency  $\Omega' \gg \Omega$ , and so it is able to sustain accretion due to repeated gravitational instability because  $\tau_c \gtrsim 3\Omega'^{-1}$ .

When  $\tau_c \gtrsim 3\Omega^{-1}$ , the outcome is similar to that of the standard run: repeated local cycles of cooling, instability, and shock heating. According to the analytic theory of §3,  $\alpha = ((9/4)\Omega\tau_c\gamma(\gamma - 1))^{-1}$  in this regime. Figure 6 shows  $\alpha$  vs.  $\tau_c$  for  $\tau_c > 3\Omega^{-1}$ . The points are measurements from numerical experiments; the solid line is the analytic result. The numerical experiments give slightly high values, for reasons discussed in §4.1.

### 4.3. Locality of Angular Momentum Transport

The preceding discussion is predicated on the idea that gravitational instability can be studied in a local model. It has been argued by Balbus & Papaloizou (1999) (hereafter BP) that the long-range nature of the gravitational force precludes such a study. Here I argue in return that, if certain conditions are fulfilled, it is self-consistent to study transport of angular momentum by gravitational instability in the local model.

The local model is an asymptotic expansion of the governing equations for a thin accretion disk to lowest order in  $\epsilon \equiv c_s/(r_0\Omega)$  in the neighborhood of a “fiducial point”. It assumes that one is studying structures on lengthscales  $\sim \epsilon r_0$ , that perturbed velocities  $\sim \epsilon r_0\Omega$ , and that the perturbed potential  $\delta\phi \sim \epsilon^2 r_0^2 \Omega^2$ . The Poisson equation is solved self-consistently in a WKB expansion (see Shu (1970) for higher order corrections). Even if  $\epsilon \ll 1$  there are several astrophysically plausible ways the local expansion might fail.

First, structure could exist in the potential on scales large compared to  $\epsilon r_0$ . For example, a bar might drive a large-scale disturbance in the neighborhood of the fiducial point. Bars cannot be generated self-consistently near the fiducial point because, as I will show below, gravitational instability only generates structure on scales comparable to  $\epsilon r_0$ . The bar must be generated elsewhere in the disk, where  $\epsilon(r) \sim 1$ . It is therefore a condition for validity of the local model that such large-scale external forcing be absent.

Second, subtler structures may exist in the velocity field, surface density, or pressure on scales larger than  $\epsilon r_0$ . For example, BP have argued that gravitational instability can extract energy from differential rotation, then transform it into waves that propagate over distances large compared to  $\epsilon r_0$  before dissipating. Such long-range coupling would invalidate a local treatment. While this is a live and interesting possibility for all types of disk turbulence, BP use linear theory to argue that self-gravitating disks are qualitatively different.

Global numerical experiments that contain large scale gradients in disk properties could falsify or confirm BP’s hypothesis regarding wave transport in self-gravitating disks, but they are beyond the scope of this paper. Here I will briefly revisit linear theory to show that self-gravitating disks are not qualitatively different from nonself-gravitating disks. I will then use the outcome of the numerical experiments to show that long-range correlations in surface density, which might be expected to develop in the presence of substantial wave transport, are not present.

Consider a density wave in a razor-thin Keplerian disk. The disk structure varies only on a scale  $r$ , and  $\epsilon(r) \ll 1$ . The wave  $\propto \exp(i(\int dr' k_r(r') + im\phi - i\omega t))$ , where  $k_r r \gg 1$  and  $m/(k_r r) \ll 1$ . The WKB dispersion relation is  $(\omega - m\Omega)^2 \equiv \nu^2 = \Omega^2 - 2\pi G \Sigma_0 |k_r| + c_s^2 k_r^2$ . The doppler-shifted frequency  $\nu^2$  has a minimum at  $|k_r| = k_{cr} \equiv \Pi G \Sigma_0 / c_s^2$ . Then the radial energy flux density, referred to an inertial frame, is

$$F_{E,wave} = \frac{1}{2} \delta\Sigma c_s^2 \left( \frac{\nu + m\Omega}{k_r} \right) \left( \frac{\delta\Sigma}{\Sigma_0} \right) \left( 1 - \frac{k_{cr}}{|k_r|} \right) \quad (22)$$

(Shu (1970); Goldreich & Tremaine (1979)). This is the full wave energy flux. BP’s “anomalous flux”, by comparison, is the gravitational component of the energy flux measured in a corotating frame. Shutting off self-gravity is equivalent to taking  $k_{cr} \rightarrow 0$  in eq.(22). Evidently the wave energy flux does not change qualitatively in this limit.

Wave energy fluxes may nonetheless be present. If they are to change disk structure significantly, however, they must be of the same order as the turbulent energy flux  $F_{E,wave} \equiv (3/2)\alpha\Sigma c_s^2 r\Omega$ . If I assume that  $\delta\Sigma \sim \Sigma_0$ ,  $Q \sim 1$ , and  $k \sim k_{cr}$ , and drop factors of order unity, I find that  $|F_{E,wave}/F_{E,turb}| \sim (m/\alpha)(c_s/(r\Omega))$  (for acoustic waves in a nonself-gravitating disk,  $c_s/(r\Omega)$  is replaced by  $1/(|k_r|r)$ ). Thus for

$$\frac{m}{\alpha} \gtrsim \frac{c_s}{r\Omega} \quad (23)$$

the wave energy flux is as important as the turbulent energy flux.

To proceed further one can only consider the plausibility of a large amplitude, high- $m$  wave propagating over significant distances in the disk. Here are two arguments against this. First, a density wave can only propagate a distance  $\sim r/m$  before it turns into an acoustic wave ( $k_r c_s \gtrsim \Omega$ ). In a finite thickness disk this corresponds to a wavelength smaller than a scale height. If the disk is stratified three-dimensional effects will modify the wave (e.g. Ogilvie & Lubow (1999)), and the wave is likely to steepen, shock, and dissipate. Second, the gravito-turbulent state contains fluctuations that emit, scatter, and absorb waves. If scattering and absorption are strong, as they are here, coherent signals are destroyed. Under these circumstances it seems unlikely that energy will be transmitted over large scales by waves.

What can the numerical models tell us about the locality of angular momentum transport in self-gravitating disks? I have used two methods to assess the locality of structure in the nonlinear outcome of my models. In the first analysis, I calculate the dimensionless autocorrelation function of the surface density,  $\xi$  :

$$\xi(\mathbf{r}) = -1 + \frac{1}{\langle \Sigma \rangle^2 L^2} \int d^2x' \Sigma(\mathbf{r} + \mathbf{r}')\Sigma(\mathbf{r}'). \quad (24)$$

Coherent wave trains would appear as large-scale correlations in the surface density. Figures 7 and 8 show the autocorrelation function averaged from a series of 5 snapshots at  $t = (20, 40, 60, 80, 100)\Omega^{-1}$ . Figure 7 shows the spatial structure of the correlation function from a run with  $L = 640G\Sigma/\Omega^2$  and  $N = 1024$ . Evidently density correlations are concentrated in a region that is much smaller than the size of the model. Figure 8 shows cuts through the correlation function (along the rays marked “short axis” and “long axis” in Figure 7) that confirm this quantitatively.

Also shown in Figure 8 is the autocorrelation function for a run with  $L = 320G\Sigma/\Omega^2$  and  $N = 512$  (the same spatial resolution as the larger model). Differences between the smaller and larger model result are small and attributable to sampling noise. The correlation function thus appears to depend only weakly on  $L$ , at least for  $L > 320G\Sigma/\Omega^2$  and  $\tau_c = 10\Omega^{-1}$ . This argues that surface density structure is locally determined.

In a second analysis, I have calculated which Fourier components of the surface density dominate the gravitational shear stress. Figure 9 shows the quantity

$$\frac{d\alpha_G}{dk} = \frac{2}{3\langle \Sigma c_s^2 \rangle} \int k d\phi \frac{\pi G k_x k_y |\Sigma_{\mathbf{k}}|^2}{2k^3}. \quad (25)$$

Here  $\phi$  is an angular coordinate in Fourier space. This is the contribution to the gravitational shear stress from Fourier components of the surface density in the annulus between  $k$  and  $k + dk$ . The result is calculated from a model with  $L = 640G\Sigma/\Omega^2$  and  $N = 1024$ . Fully 90% of the angular momentum transport comes from wavenumbers with  $k > 5(2\pi/L)$ . Thus wavelengths significantly smaller than the model size dominate the shear stress.

Figure 9 can be used to estimate how cool a disk must be for the local model to be applicable. If the wavenumber  $k_{pk}$  of the maximum in  $d\alpha_G/dk$  is to satisfy  $k_{pk}r/(2\pi) \ll 1$ , then one needs

$$\frac{c_s}{r\Omega} \ll 0.12. \quad (26)$$

where I have used  $(2\pi/k_{pk}) \approx 64G\Sigma/\Omega^2$  and  $\langle c_s \rangle = 7.7G\Sigma/\Omega$ . YSO disks have  $H/r \simeq 0.1$  and so are at best marginally described by a local approximation. Some AGN disk models are much thinner and thus may be accurately described with a local model. In disks that violate condition (26), such as those studied by Laughlin & Różyczka (1996), global effects can be important.

#### 4.4. Effect of Resolution

Most experiments described in this paper have been run at multiple resolution to determine convergence. The resolution at which convergence is achieved depends on what is being measured. Consider the convergence of  $\alpha$ , as measured numerically. Figure 10 shows  $\alpha$ , averaged over the final  $80\Omega^{-1}$  of the run, in a model with  $L = 320G\Sigma/\Omega^2$  and  $N = 32, 64, \dots, 1024$ . Evidently  $\alpha$  has converged. Investigation of models of different physical size shows that convergence requires resolution of a fixed physical scale which is  $\approx G\Sigma/\Omega^2$ .

#### 4.5. Length of Run

The autocorrelation analysis of §4.3 shows that large-scale structures are not established on a dynamical timescale. Suppose, however, that gravito-turbulence acts as a viscosity on long-wavelength modes. Then there is the possibility of a secular instability analogous to that of viscous, self-gravitating disks discussed by Lynden-Bell & Pringle (1974), and also Gor’kavvi et al. (1989); Willerding (1992); Schmit & Tscharnuter (1995); Gammie (1996b). These instabilities grow on the viscous timescale,  $\sim (\lambda/(2\pi H))^2(\alpha\Omega)^{-1}$ .

As a preliminary test for secular instability, I have integrated two large ( $L = 160G\Sigma/\Omega^2$ ), high-resolution ( $N = 512$ ) models for  $10^3\Omega^{-1}$ . One model had  $\tau_c = 40\Omega^{-1}$ , the other  $\tau_c = 10\Omega^{-1}$ .

The energy evolution of the latter is shown in Figure 11. There is no clear trend in any of the energy components over the course of the simulation. The  $\tau_c = 40\Omega^{-1}$  run is similar. If secular instability is present, it grows only on longer timescales.

Returning to the analogy with secular instability of viscous, self-gravitating disks, an integration over a time  $t_f$  can be regarded as a test for secular instability over wavelengths  $\lambda \lesssim \lambda_c = 2\pi H \sqrt{\alpha t_f \Omega}$ . For the integrations described here  $\lambda_c \approx 30G\Sigma/\Omega^2$ . Thus longer integrations, although expensive, hold the possibility of interesting results.

## 5. Implications

What are the implications for the structure of disks around YSOs? Although our results are not rigorously applicable, since  $H/r$  is typically of order 0.1–0.2 in the outer parts of YSO disks, they may provide a guide to the relevant physics.

In models of unilluminated YSO disks (Ruden & Pollack 1991; Gammie 1996a)  $Q$  approaches unity at a radius  $r \sim 30$  AU, where the temperature is  $\approx 20$  K. Illumination can change  $Q(r)$  dramatically (Kenyon & Hartmann (1987); for more recent models see, e.g., D’Alessio et al. (1999); Bell (1999)). For sufficiently strong illumination, or sufficiently low mass disk, the entire disk is gravitationally stable. As the illumination is reduced some radii become gravitationally unstable.

At gravitationally unstable radii there are two possible outcomes. If the cooling time of the disk is sufficiently long ( $\tau_c \gtrsim 3\Omega^{-1}$ ), then gravitationally driven turbulence will simply enhance the shear stress above that available from other sources, such as MHD turbulence. This shear stress is generated in a region of order  $64G\Sigma/\Omega^2$  across and all the numerical evidence is consistent with its being locally determined and treatable as an  $\alpha$  viscosity (but only if  $H/r \ll 0.1$ ). Recurrent instability and shock heating maintain  $\langle Q \rangle \approx 2.4$ , somewhat larger than the value required for axisymmetric stability.

If, on the other hand, the cooling time in the disk is short ( $\Omega\tau_c \lesssim 3$ ), the outcome is dramatically different. Such short cooling times might be found in a disk heated mainly by external illumination that is suddenly switched off (for example, in YSO disks, as an FU Orionis outburst turns off). In this case the model disk fragments, as suggested by Shlosman & Begelman (1989) in the context of AGN disks. The long-term evolution of these systems is uncertain because it is intrinsically global; the fragments undergo collisional agglomeration within bands in radius. Clearly one possible outcome is the formation of gas giant planets (e.g. Boss (1997) and references therein), but the final mass of the object depends on the global evolution. Global models including more realistic cooling functions (such as those developed by Nelson et al. (2000)), and external illumination, are clearly desirable.

AGN disk models also generally become gravitationally unstable at large radius (Shlosman & Begelman 1989). They typically have  $H/r \ll 0.1$  and so the local approximation is more applicable

than in YSO disks. Typically at large radius their cooling time is short (equivalently: the  $\alpha$  required to prevent instability becomes large). The numerical models presented here suggest that fragmentation, and perhaps star formation, is likely under these circumstances.

I am grateful to Jeremy Goodman, Steve Balbus, Ramesh Narayan, and John Papaloizou for their comments. This work was supported by NASA grant NAG 52837, NAG 58385, and a grant from the University of Illinois Research Board.

## REFERENCES

- Adams, F.C., & Lin, D.N.C. 1993, in *Protostars and Planets III* (Tucson: Arizona), 721
- Adams, F.C., Ruden, S.P., & Shu, F.H. 1989, *ApJ*, 347, 959
- Anthony, D.M. & Carlberg, R.G. 1988, *ApJ*, 332, 637
- Balbus, S.A. & Papaloizou, J.C.B. 1999, *ApJ*, 521, 650
- Bell, K.R. 1999, *ApJ*, 526, 411
- Boss, A.P. 1997, *Science*, 276, 1836
- Boss, A.P. 1998, *ApJ*, 503, 923
- Carlberg, R.G., & Freedman, W.L. 1985, *ApJ*, 298, 486
- D'Alessio, Paola, Calvet, N., Hartmann, L., Lizano, S., & Cantó, J. 1999, *ApJ*, 527, 893
- Gammie, C.F. 1996a, *ApJ*, 457, 355
- Gammie, C.F. 1996b, *ApJ*, 462, 725
- Gammie, C.F., Narayan, R., & Blandford, R. 1999, *ApJ*, 516, 177
- Goldreich, P. & Lynden-Bell, D. 1965, *MNRAS*, 130, 125
- Goldreich, P. & Tremaine, S. 1979, *ApJ*, 233, 857
- Gor'kavyi, N. N., Polyachenko, V. L., & Fridman, A. M. 1989, *Sov. Astron. Lett.* 16, 79
- Hawley, J.F., Gammie, C.F., & Balbus, S.A. 1995a, *ApJ*, 440, 742
- Hunter, C. 1964, *ApJ*, 139, 570
- Kennicutt, R.C. 1989, *ApJ*, 344, 685
- Kenyon, S., & Hartmann, L., 1987, *ApJ*, 323, 714
- Laughlin, G., & Różyczka, M. 1996, *ApJ*456, 279
- Lasota, J.-P. et al. 1996, *ApJ*, 462, 142
- Lin, D.N.C., & Pringle, J.E. 1987, *MNRAS*, 225, 607
- Lin, D.N.C., & Pringle, J.E. 1990, *ApJ*, 358, 515
- Lynden-Bell, D. 1966, *The Observatory*, 86, 57
- Lynden-Bell, D., & Kalnajs, A.J. 1972, *MNRAS*, 157, 1

- Lynden-Bell, D., & Pringle, J.E. 1974, MNRAS, 168, 603
- Masset, F. 1999, astro-ph/9910390
- Miyoshi, M. et al. 1995, Nature, 373, 127
- Nelson, A.F., Benz, W., & Adams, F.C., Arnett, D. 1998, ApJ, 502, 342
- Nelson, A.F., Benz, W., & Ruzmaikina, T. 2000, ApJ, 529, 357
- Ogilvie, G.I., & Lubow, S.H. 1999, ApJ, 515, 767
- Owen, T., et al. 1999, Nature, 402, 269
- Pickett, B.K., Cassen, P., Durisen, R.H., & Link, R. 2000, ApJ, 529, 1034
- Paczyński, B. 1978, Act. Astron., 28, 91
- Ruden, S.P., & Pollack, J.B. 1991, ApJ, 375, 740
- Schmit, U., & Tscharnuter, W.M. 1995, Icarus, 115, 304
- Sellwood, J.A., & Carlberg, R.G. 1984, ApJ, 282, 61
- Shakura, N.I., & Sunyaev, R.A. 1973, A&A, 24, 337
- Shlosman, I., & Begelman, M. 1989, ApJ, 341, 685
- Shlosman, I., & Begelman, M., & Frank, J. 1990, Nature, 345, 679
- Shu, F. 1970, ApJ, 160, 99
- Tomley, L., Cassen, P., & Steiman-Cameron, T. 1991, ApJ, 382, 530
- Tomley, L., Steiman-Cameron, T.Y. & Cassen, P., 1994, ApJ, 422, 850
- Toomre, A. 1964, ApJ, 139, 1217
- Toomre, A., & Kalnajs, A. 1991, in Dynamics of Disc Galaxies, ed. B. Sundelius (Sweden, Göteborg University), 341
- Willerding, E. 1992, Earth, Moon, & Plan., 56, 173
- Wisdom, J., & Tremaine, S. 1988, AJ, 95, 925
- Yang, S., Durisen, R.H., Cohn, H.S., Imamura, J.N., & Toman, J. 1991, Icarus, 91, 14

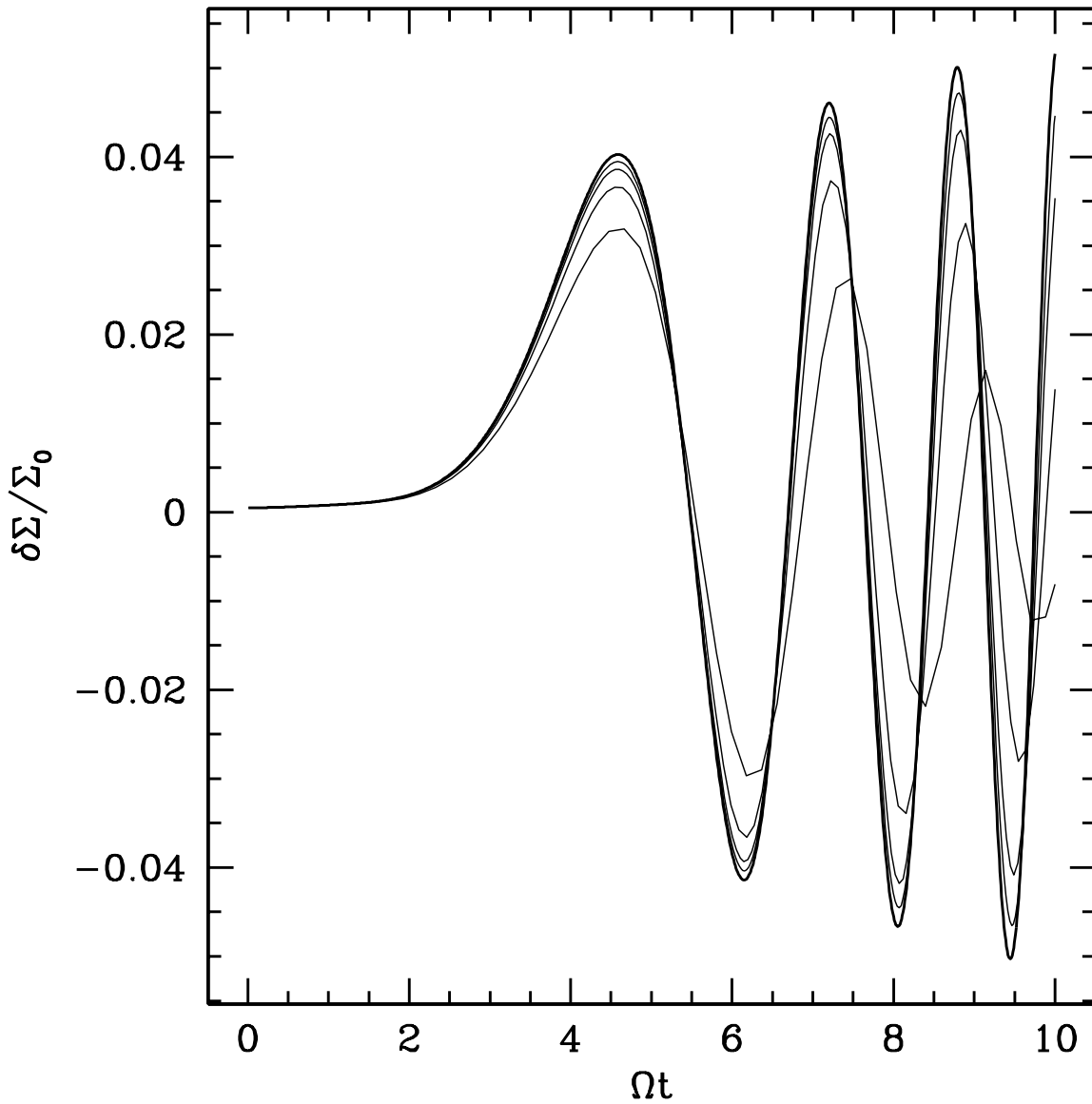


Fig. 1.— Evolution of the amplitude, in surface density, of a shearing Fourier component. The heavy solid line shows the linear theory result. The light lines show measurements from a numerical experiment with  $N = 32$  (poorest agreement with linear theory),  $N = 64, \dots, 256$ .

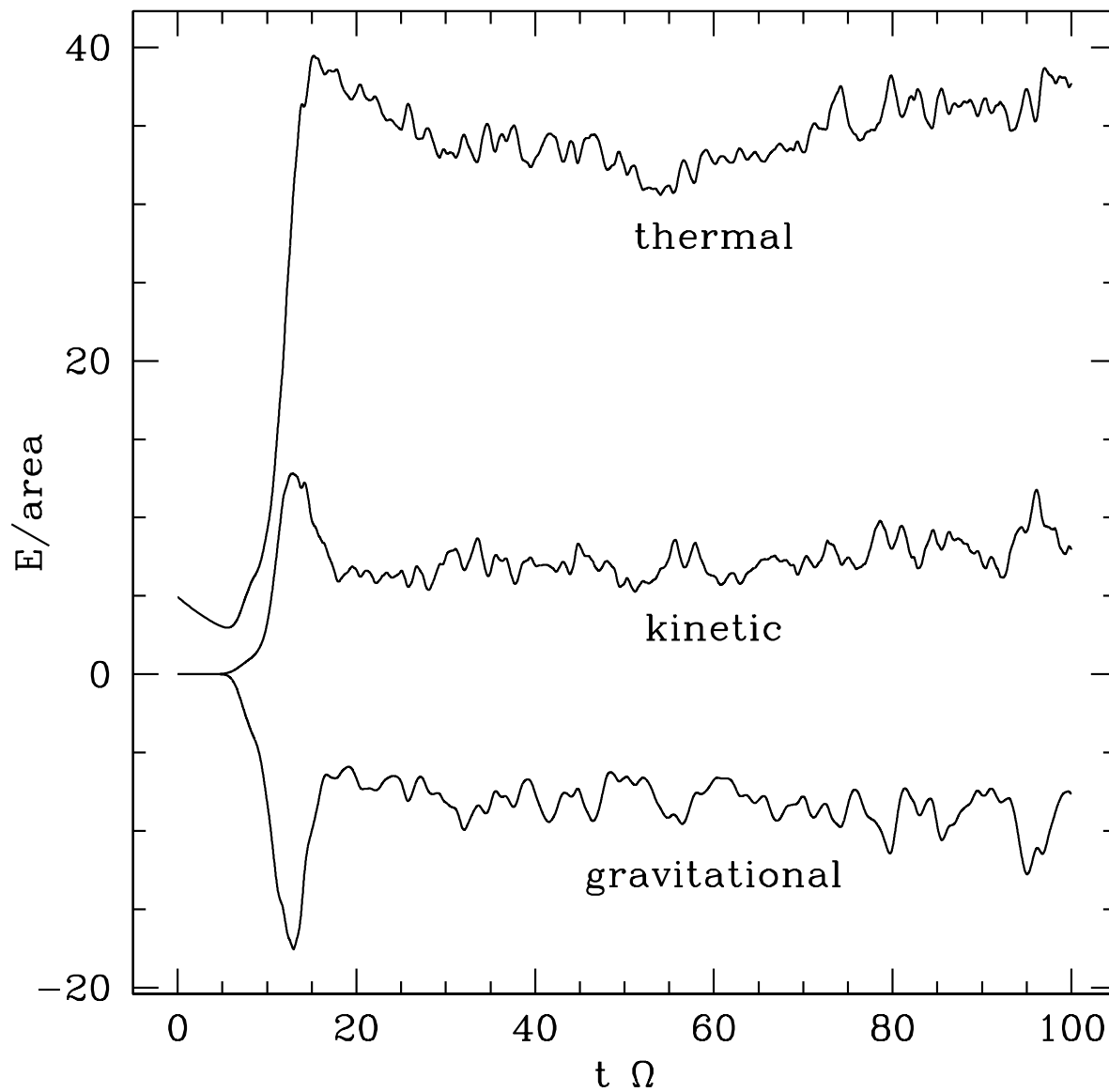


Fig. 2.— Evolution of the kinetic, gravitational, and thermal energy per unit area, normalized to  $G^2\Sigma^3/\Omega^2$ , in the standard run, which has  $L = 320G\Sigma/\Omega^2$ ,  $N = 1024$ , and  $\tau_c = 10\Omega^{-1}$ .

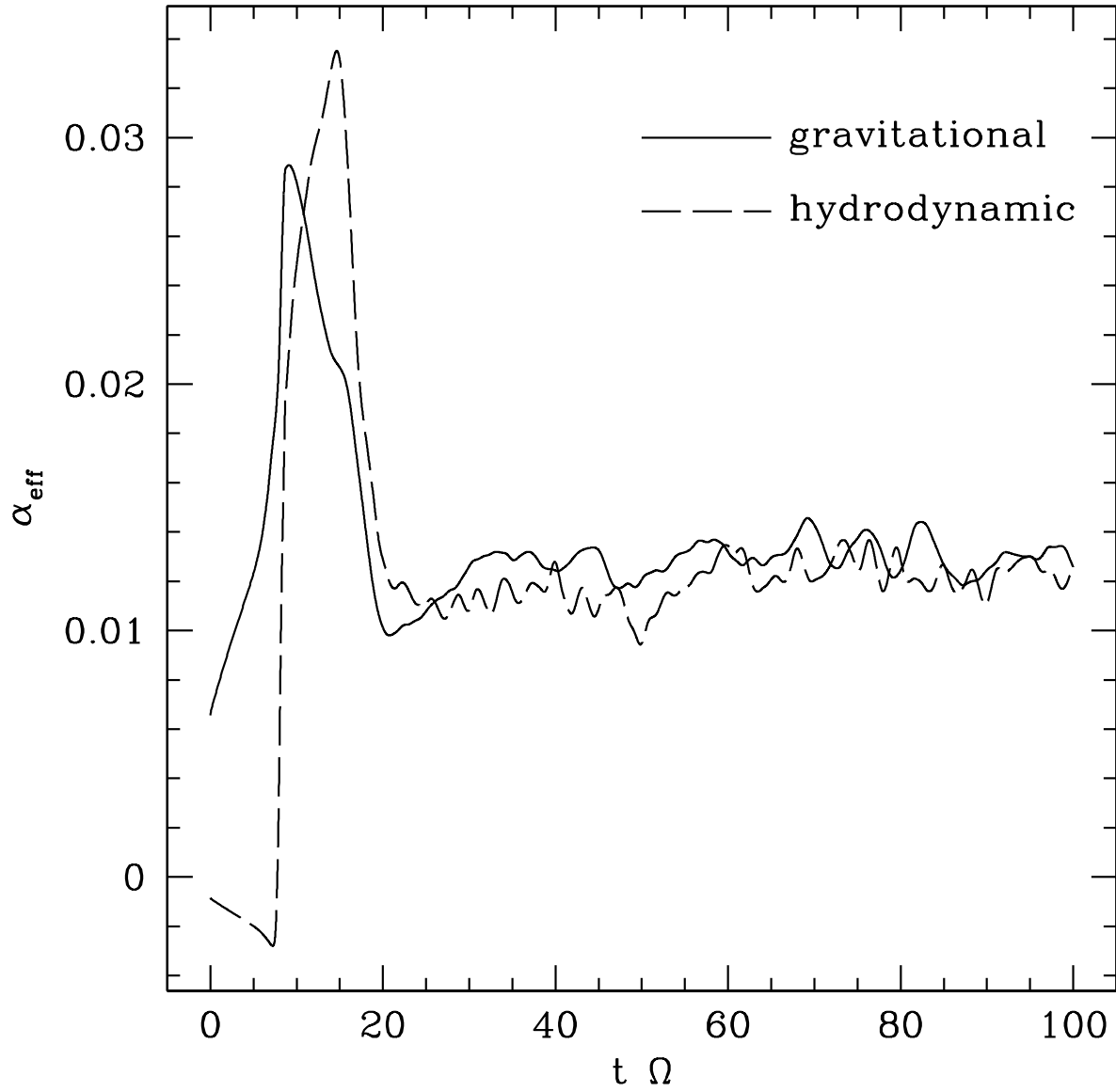


Fig. 3.— Evolution of the gravitational and hydrodynamic pieces of  $\alpha$  in the standard run. The curves have been boxcar smoothed over an interval  $10\Omega^{-1}$  to make the plot readable.

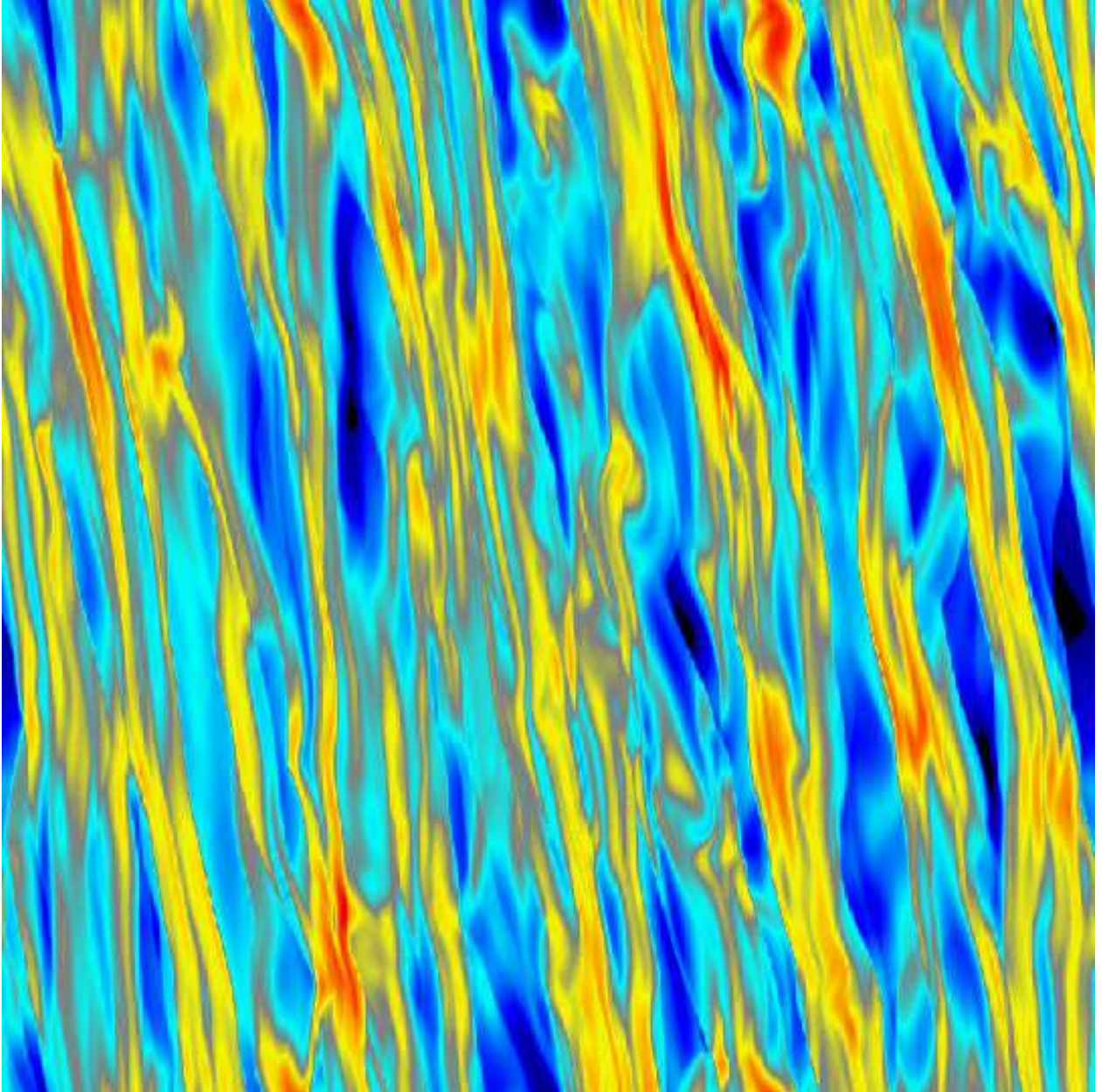


Fig. 4.— Map of surface density at  $t = 50\Omega^{-1}$  in the standard run. Black is low density and red is high density.

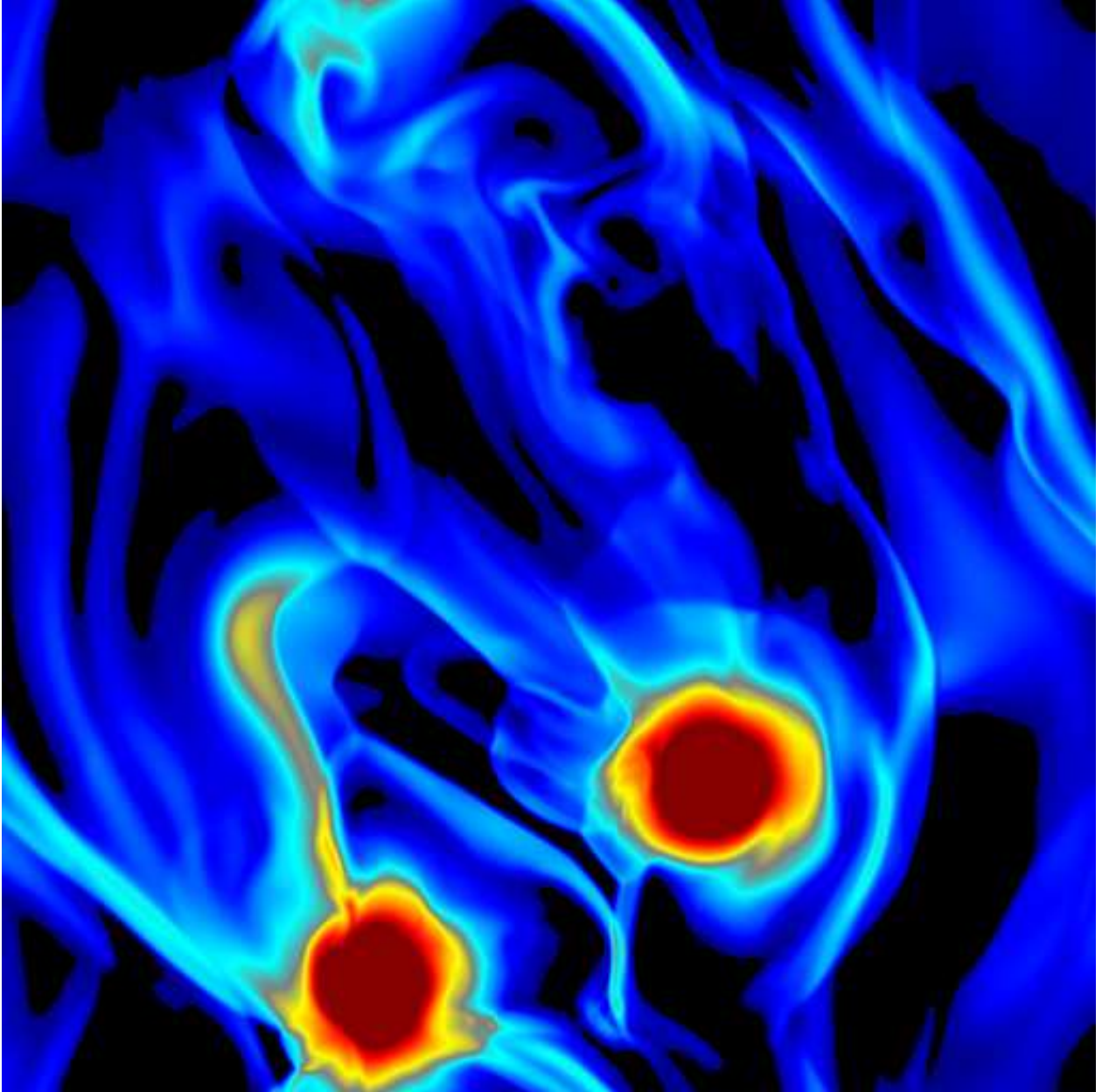


Fig. 5.— Map of surface density in a run with  $\tau_c = 2\Omega^{-1}$ . Black is low density and red is high density. The disk has fragmented and formed two bound objects. These objects eventually collide and coalesce.

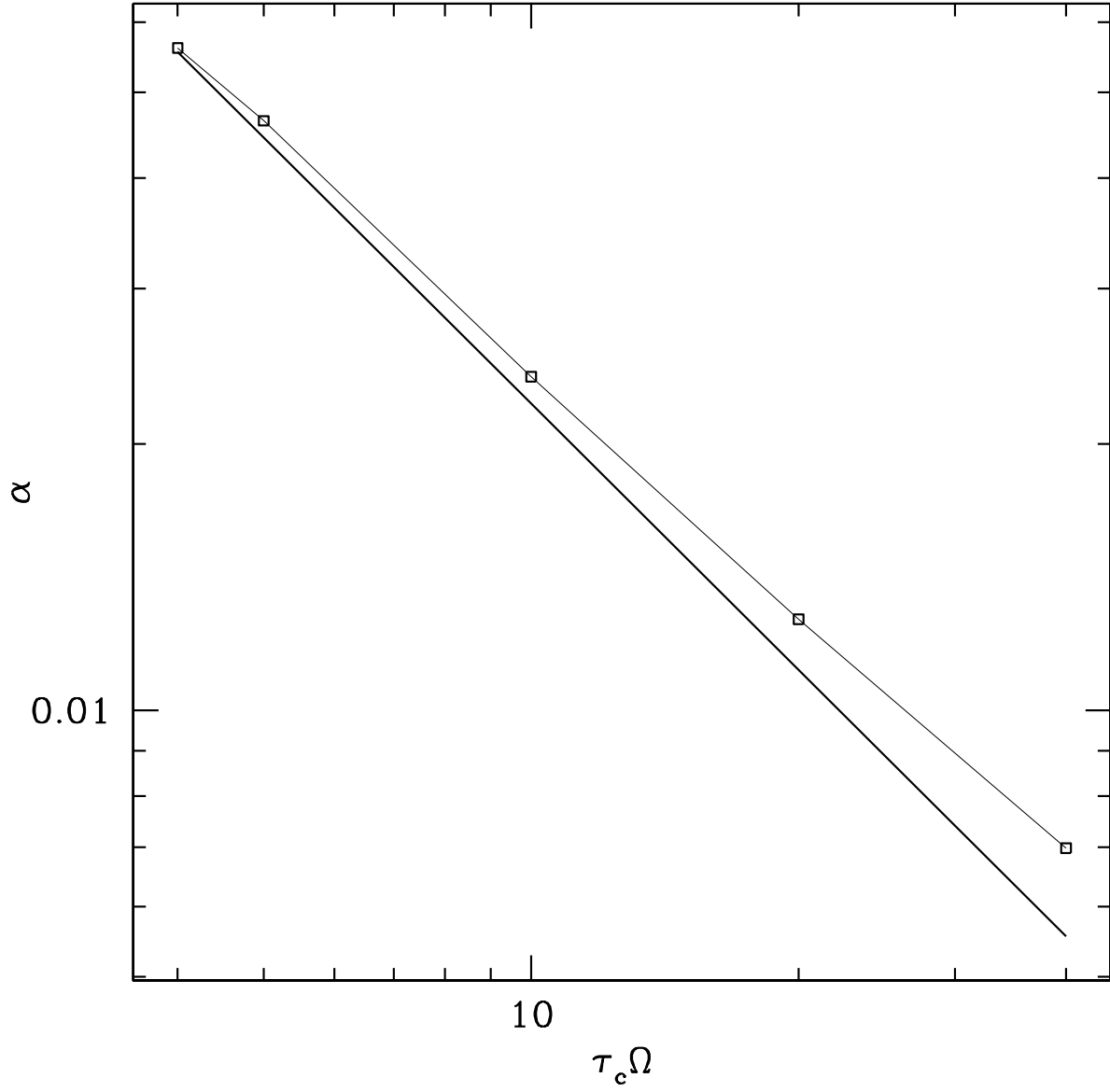


Fig. 6.— Time-averaged  $\alpha$  for a series of runs with  $4 \leq \tau_c \Omega \leq 40$  (points) and the analytic scaling of §3 (solid line).

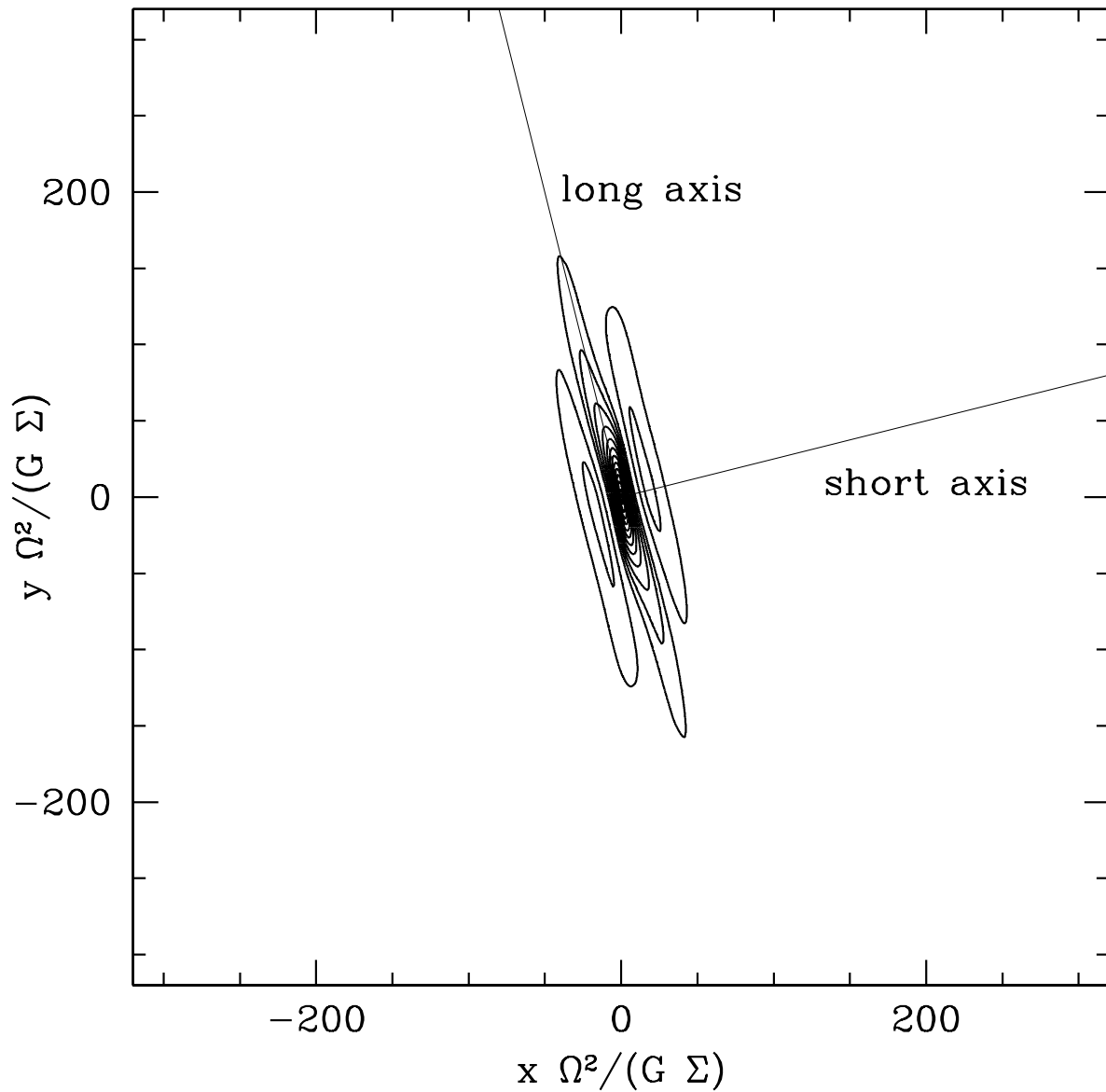


Fig. 7.— Dimensionless autocorrelation function of the surface density, averaged over a series of snapshots from a run with  $L = 640G\Sigma/\Omega^2$  and  $N = 1024$ . The lines show the cuts along which the correlation function is sampled for Figure 8. Contours are  $-0.05, -0.025, 0.025, 0.05, 0.075, \dots 0.3$ .

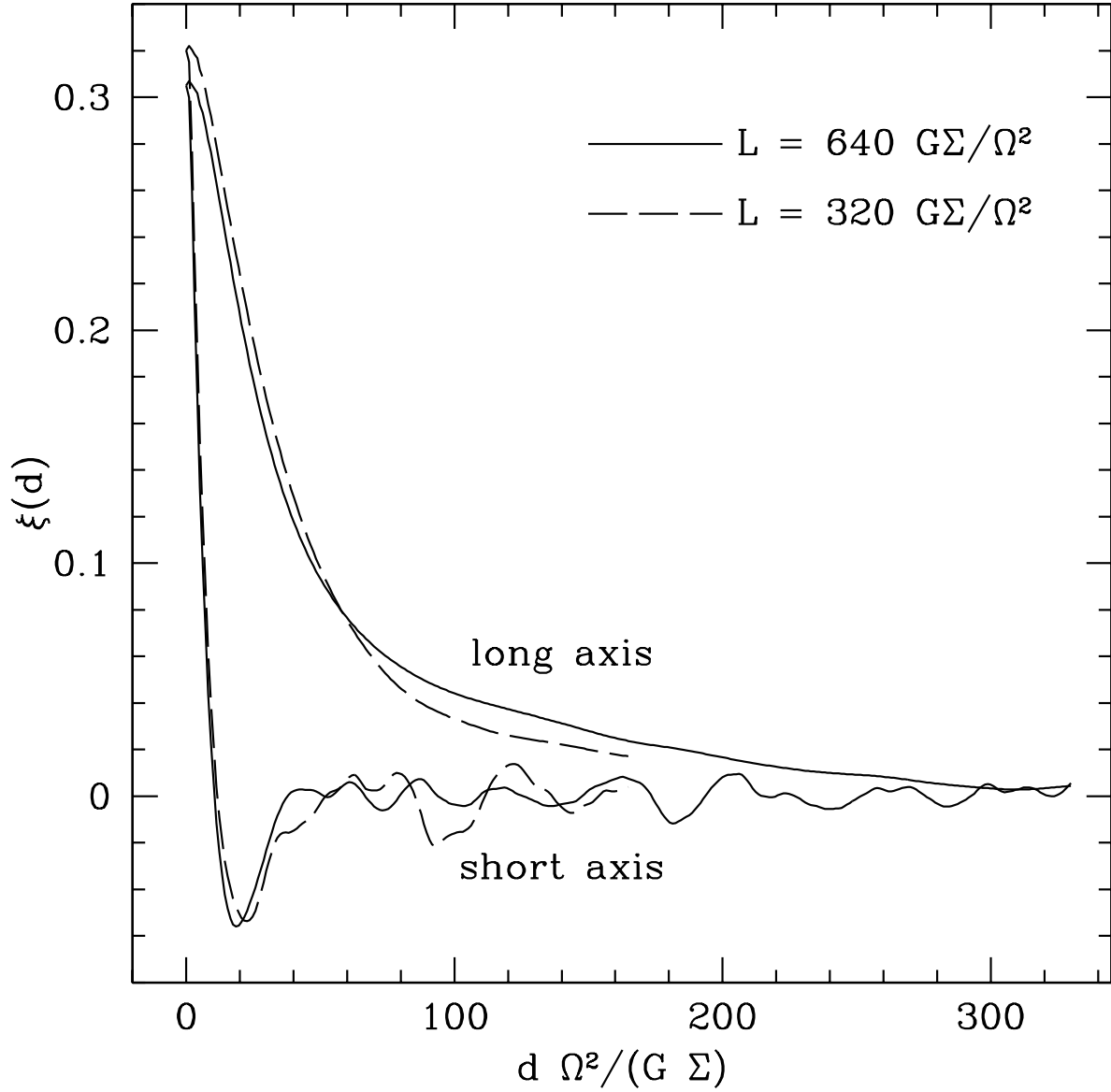


Fig. 8.— The dimensionless autocorrelation function of the surface density, averaged over a series of snapshots from a run with  $L = 640 G \Sigma / \Omega^2$  and  $N = 1024$ . The correlation function is sampled along the lines shown in Figure 7. The dashed line is for a run with  $L = 320 G \Sigma / \Omega^2$ ; the solid line is for a run with  $L = 640 G \Sigma / \Omega^2$ .

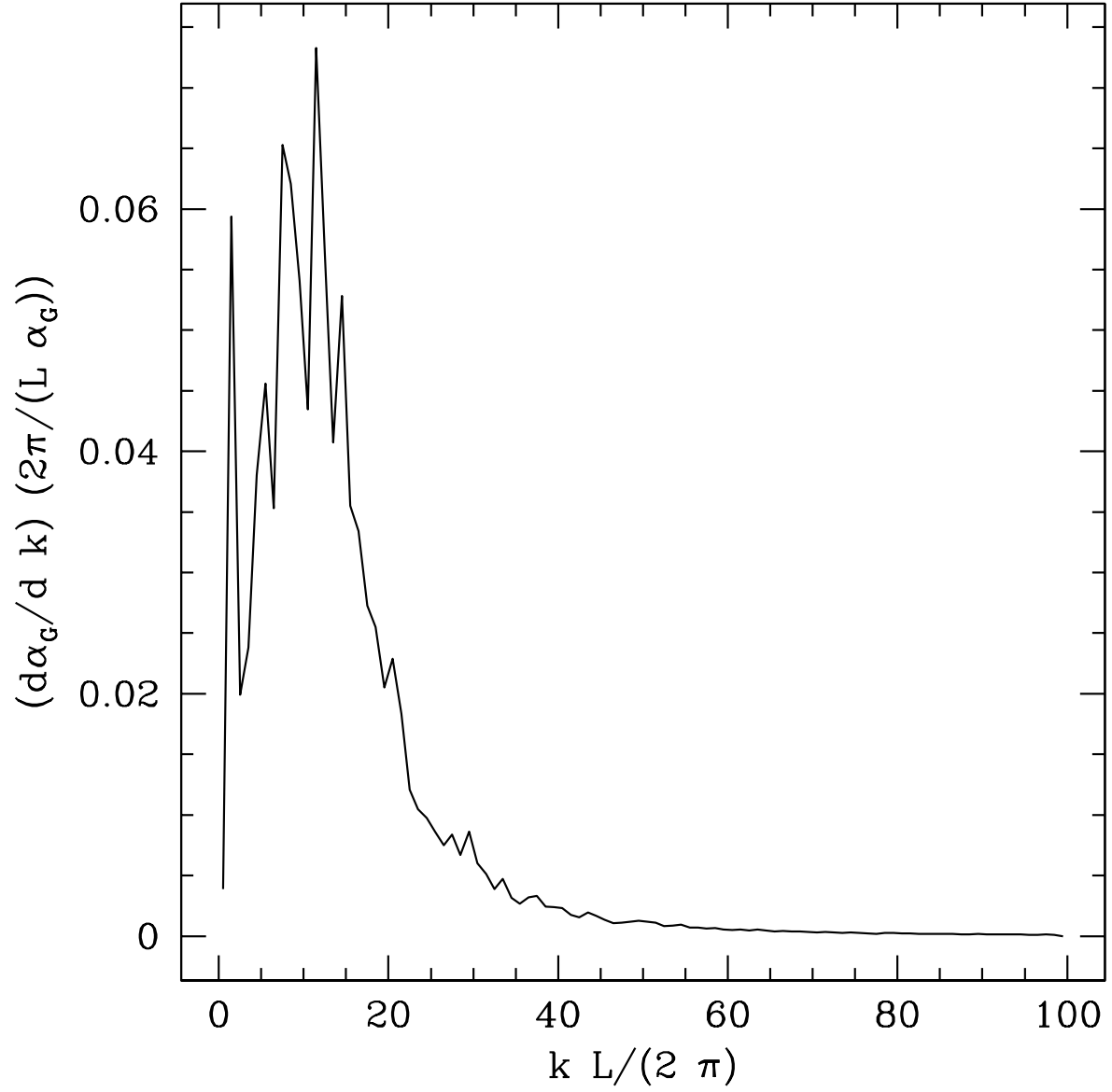


Fig. 9.— Distribution of the gravitational component of  $\alpha$  over  $|\mathbf{k}|$ , from a run with  $L = 640G\Sigma/\Omega^2$  and  $N = 1024$ . Fully 90% of the shear stress comes from wavelengths  $\lambda < L/5$ .

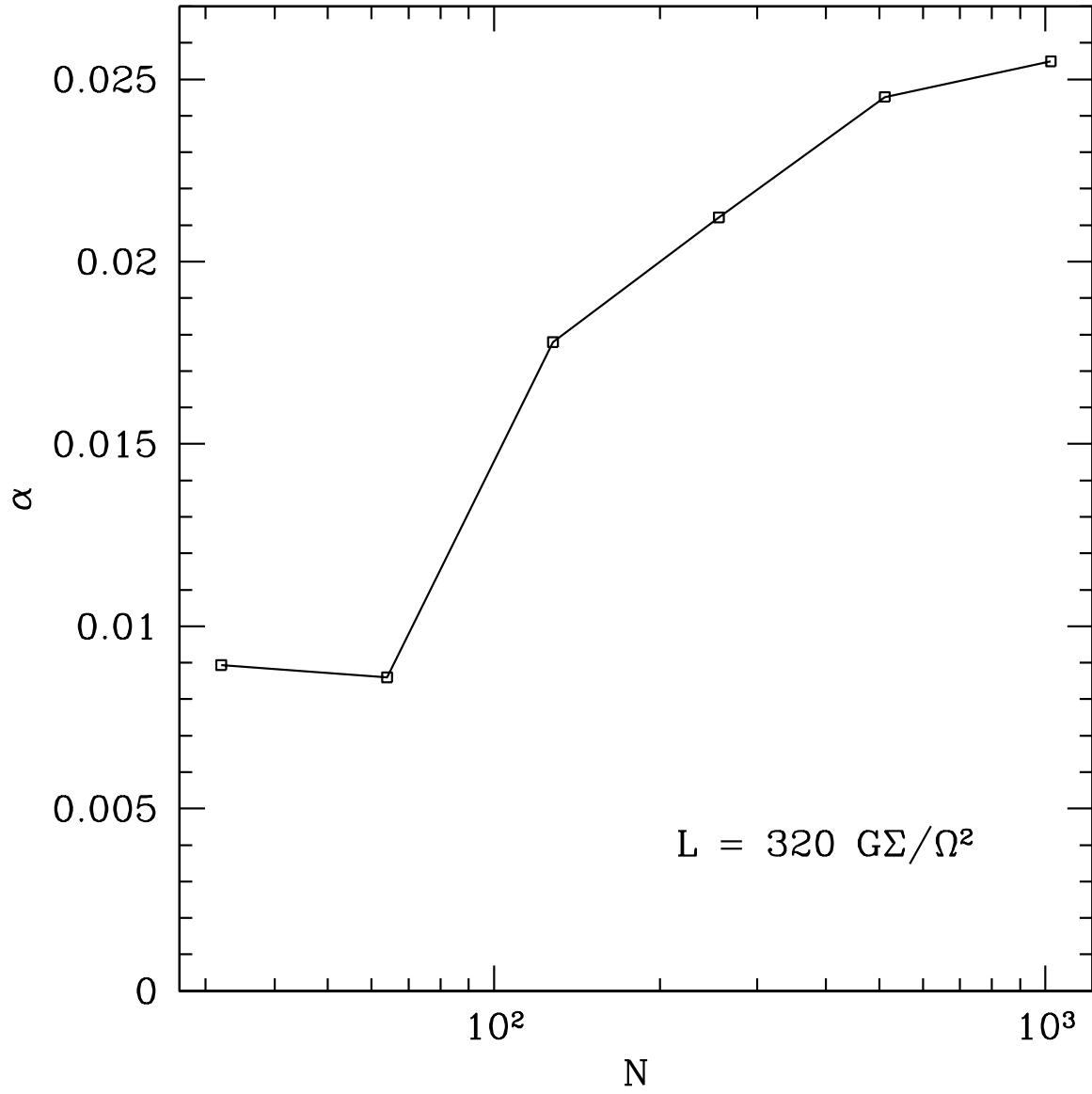


Fig. 10.— Shear stress  $\alpha$  vs. numerical resolution  $N$ , for runs with  $L = 320G\Sigma/\Omega^2$  and  $\tau_c = 10\Omega^{-1}$ .

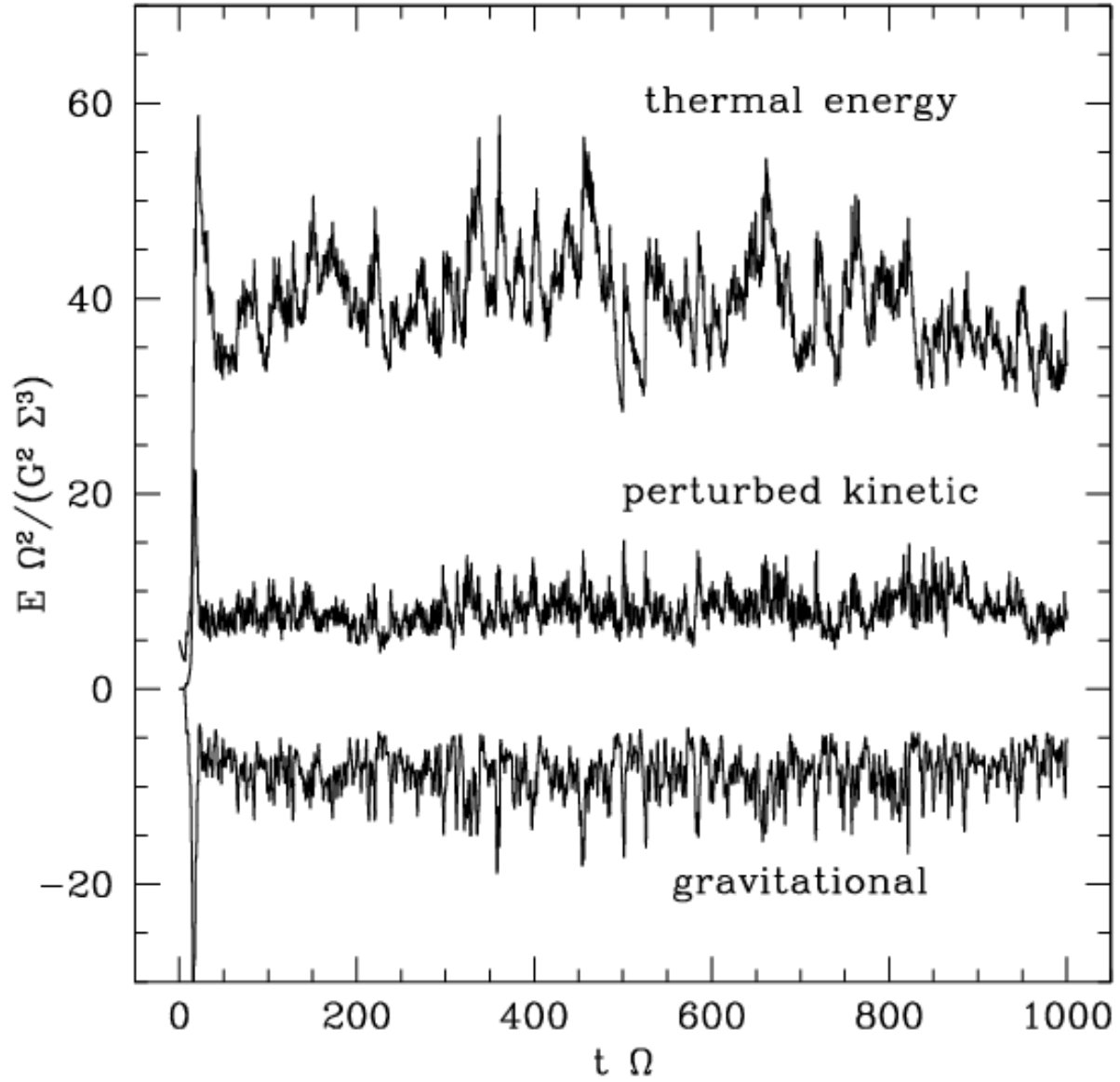


Fig. 11.— Evolution of thermal, kinetic, and gravitational energy in a long ( $10^3\Omega^{-1}$ ) run, with  $\tau_c = 10\Omega^{-1}$ . No clear trend, indicative of a secular instability, is present.